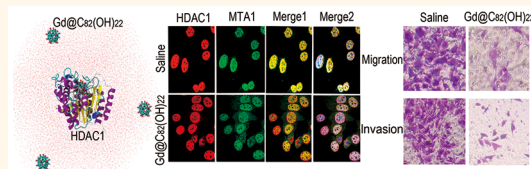


# Gd–Metallofullerenol Nanomaterial Suppresses Pancreatic Cancer Metastasis by Inhibiting the Interaction of Histone Deacetylase 1 and Metastasis-Associated Protein 1

Yuanming Pan,<sup>†</sup> Liming Wang,<sup>‡</sup> Seung-gu Kang,<sup>§</sup> Youyong Lu,<sup>||</sup> Zaixing Yang,<sup>†</sup> Tien Huynh,<sup>§</sup> Chunying Chen,<sup>‡</sup> Ruhong Zhou,<sup>\*,§,✉</sup> Mingzhou Guo,<sup>\*,†</sup> and Yuliang Zhao<sup>\*,‡</sup>

<sup>†</sup>Department of Gastroenterology & Hepatology, Chinese PLA General Hospital, #28 Fuxing Road, Beijing 100853, China, <sup>‡</sup>CAS Key Laboratory for Biomedical Effects of Nanomaterials and Nanosafety, National Center for Nanoscience and Technology and Institute of High Energy Physics, Chinese Academy of Sciences, Beijing 100190, China, <sup>§</sup>Computational Biology Center, IBM Thomas J. Watson Research Center, 1101 Kitchawan Road, Yorktown Heights, New York 10598, United States, <sup>||</sup>Laboratory of Molecular Oncology, Key Laboratory of Carcinogenesis and Translational Research (Ministry of Education), Peking University Cancer Hospital & Institute, Beijing 100142, China, and <sup>†</sup>Institute of Quantitative Biology and Medicine, SRMP and RAD-X, Soochow University, Suzhou 215123, China

**ABSTRACT** The treatment of pancreatic cancer frequently fails due to local recurrence and hepatic metastasis. Our previous study found that Gd@C<sub>82</sub>(OH)<sub>22</sub> can suppress pancreatic cancer by inhibiting MMP-2/9 expression. In this study, we further explored the epigenetic mechanism of Gd@C<sub>82</sub>(OH)<sub>22</sub> in human pancreatic cancer metastasis. Gd@C<sub>82</sub>(OH)<sub>22</sub> suppressed tumor metastasis through down-regulation of metastasis-associated protein 1 (MTA1), HDAC1, HIF-1 $\alpha$ , and MMP-2/9 and up-regulation of reversion-cysteine protein with the Kazal motif (RECK). The level of acetylation was increased in the promoter region of the RECK gene after Gd@C<sub>82</sub>(OH)<sub>22</sub> treatment. The interaction of MTA1, HDAC1, and HIF-1 $\alpha$  was inhibited by Gd@C<sub>82</sub>(OH)<sub>22</sub>. Furthermore, large-scale molecular dynamics simulations revealed Gd@C<sub>82</sub>(OH)<sub>22</sub> could serve as an effective HDAC inhibitor to the protein–protein association between HDAC1 and MTA1, especially through MTA1's SANT and ELM2 dimerization domains. Our findings implicate Gd@C<sub>82</sub>(OH)<sub>22</sub> as a novel HDAC inhibitor acting to increase RECK expression by suppressing the MTA1/HDAC1 co-repressor complex. Gd@C<sub>82</sub>(OH)<sub>22</sub> may serve as a potential HDAC1 inhibitor to suppress pancreatic cancer cell invasion and metastasis both *in vitro* and *in vivo*. According to computer analysis and experimental validation, Gd@C<sub>82</sub>(OH)<sub>22</sub> activates RECK expression by inhibiting the interaction of HDAC1 and MTA1.



**KEYWORDS:** pancreatic cancer · Gd@C<sub>82</sub>(OH)<sub>22</sub> · metastasis · HDAC1 · MTA1 · HIF-1 $\alpha$  · RECK

Pancreatic cancer is a malignant disease with increasing incidence worldwide. Most treatment failures are due to local recurrence and hepatic metastasis, making it critical to understand the mechanism of metastasis for development of effective therapies.<sup>1–4</sup> Hypoxia is an essential feature of the microenvironment in solid tumors. Hypoxia-inducible factor-1 $\alpha$  (HIF-1 $\alpha$ ), metastasis-associated protein 1 (MTA1), and histone deacetylase 1 (HDAC1) are known to be induced under hypoxia.<sup>5,6</sup> Dysregulation of MTA1 and HIF-1 $\alpha$  enhances tumor metastasis and down-regulates of the reversion-cysteine protein with the Kazal motif (RECK) under hypoxia by recruiting

HDAC1.<sup>7</sup> RECK is a membrane-anchored glycoprotein that negatively regulates matrix metalloproteinases (MMPs) to inhibit tumor metastasis and angiogenesis.<sup>8–12</sup> It was suggested that HDAC inhibitors (HDACIs) suppress cancer cell invasion by up-regulating RECK.<sup>7,13,14</sup>

HIF-1 $\alpha$  is a subunit of HIF-1, a key regulator of cellular adaptive responses to hypoxia and involved in many pathways related to angiogenesis and metastasis.<sup>15–17</sup> It is usually degraded through the ubiquitin/proteasome system under normoxia. However, most pancreatic cancer cell lines express high levels of HIF-1 $\alpha$  under normoxia,<sup>18,19</sup> which reinforces the malignancy

\* Address correspondence to mzguo@hotmail.com, zhaoyuliang@ihp.ac.cn, ruhongz@us.ibm.com.

Received for review November 27, 2014  
and accepted June 17, 2015.

Published online June 17, 2015  
10.1021/nn506782f

© 2015 American Chemical Society

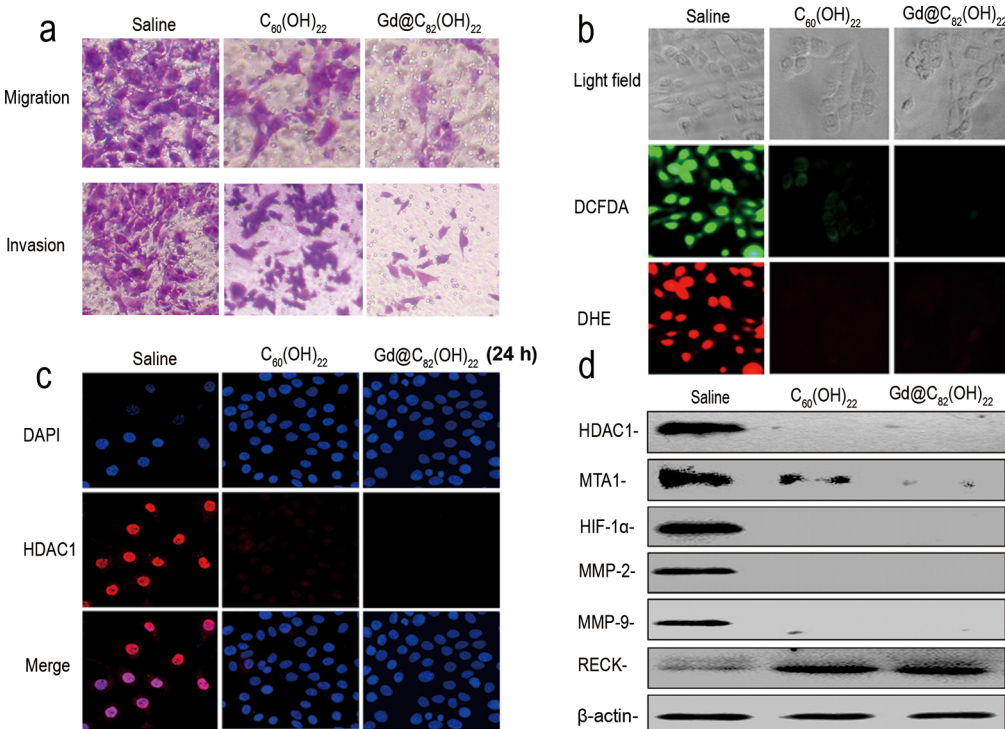


**Figure 1.**  $\text{Gd@C}_{82}(\text{OH})_{22}$  and  $\text{C}_{60}(\text{OH})_{22}$  suppress cell migration and invasion at the concentration of  $50 \mu\text{M}$  for 24 h in Panc5.04 cells. (a) Transwell assay shows that  $\text{Gd@C}_{82}(\text{OH})_{22}$  and  $\text{C}_{60}(\text{OH})_{22}$  inhibit cell migration and invasion in Panc5.04 cells. (b) Reactive oxygen species (green) and  $\text{O}_2^-$  (red) were suppressed by  $\text{C}_{60}(\text{OH})_{22}$  and  $\text{Gd@C}_{82}(\text{OH})_{22}$  in Panc5.04 cells. (c) Immunofluorescence assay shows that the expression of HDAC1 was suppressed by  $\text{C}_{60}(\text{OH})_{22}$  or  $\text{Gd@C}_{82}(\text{OH})_{22}$ . (d) Expression of HDAC1, MTA1, HIF-1 $\alpha$ , MMP-2, and MMP-9 was reduced, and the expression of RECK was increased after  $\text{C}_{60}(\text{OH})_{22}$  or  $\text{Gd@C}_{82}(\text{OH})_{22}$  treatment in Panc5.04 cells.

of pancreatic cancer. MTA1 has been regarded as a candidate metastasis-associated molecule that plays an important role in tumor invasion and metastasis by interacting with HDACs.<sup>5,20</sup> Low-level expression of MTA1 is found in various normal tissues, but the expression is increased markedly in different cancers, including pancreatic cancer.<sup>21–26</sup>

The dynamic interplay of acetylation and deacetylation governs gene expression. HDACs are overexpressed in many primary human cancers,<sup>27–30</sup> including pancreatic cancer.<sup>31–34</sup> In particular, HDAC1 is regarded as one of the important therapeutic targets in human cancer.<sup>35–37</sup> HDAC inhibitors suppress cancer cell invasion, migration, and metastasis by down-regulating HIF-1 $\alpha$  *in vitro* and *in vivo*.<sup>38,39</sup>

Fullerene and its derivatives have been widely studied in biomedical fields recently due to their unique optoelectronic and physiochemical properties. Water-soluble fullerene derivatives are regarded as free radical scavengers and antioxidants.<sup>40,41</sup> Functionalized fullerenes have also shown potential in tumor therapies, such as photodynamic therapy, photothermal treatment, and chemotherapeutics. It was recently reported that  $\text{Gd@C}_{82}(\text{OH})_{22}$  can suppress pancreatic cancer metastasis by inhibiting MMP-2/9 expression and activity.<sup>42</sup> However, the way MMP-2/9 expression was regulated is still not clear. Here, we investigated the mechanism of

$\text{Gd@C}_{82}(\text{OH})_{22}$  on epigenetic regulation of human pancreatic cancer metastasis.

## RESULTS AND DISCUSSION

**$\text{Gd@C}_{82}(\text{OH})_{22}$  Suppresses Cell Migration and Invasion by Inhibiting MMP-2/9, MTA1, HDAC1, and HIF-1 $\alpha$  Expression in Pancreatic Cancer Cells.** To understand the mechanism of  $\text{C}_{60}(\text{OH})_{22}$  and  $\text{Gd@C}_{82}(\text{OH})_{22}$  in pancreatic cancer metastasis, transwell assay, immunofluorescence, and Western blotting were employed in pancreatic cancer cells. As shown in Figure 1a, the number of migration cells (Panc5.04) is  $136 \pm 12$  versus  $45 \pm 6$  ( $P < 0.01$ ) and  $134 \pm 27$  versus  $21 \pm 3$  ( $P < 0.01$ ) before and after  $\text{C}_{60}(\text{OH})_{22}$  or  $\text{Gd@C}_{82}(\text{OH})_{22}$  treatment, respectively. The number of migration cells was reduced significantly in  $\text{C}_{60}(\text{OH})_{22}$ -treated and  $\text{Gd@C}_{82}(\text{OH})_{22}$ -treated Panc5.04 cells. The number of invasive cells is  $182 \pm 16$  versus  $66 \pm 7$  ( $P < 0.05$ ) and  $180 \pm 20$  versus  $15 \pm 6$  (Figure 1a,  $P < 0.01$ ) before and after  $\text{C}_{60}(\text{OH})_{22}$  treatment and  $\text{Gd@C}_{82}(\text{OH})_{22}$  treatment, respectively. The number of invasive cells was also reduced significantly in both  $\text{C}_{60}(\text{OH})_{22}$  and  $\text{Gd@C}_{82}(\text{OH})_{22}$  treatment. Similar results were obtained in Panc3.11 cells (Supporting Information Figure S1a,b). These results suggest that  $\text{C}_{60}(\text{OH})_{22}$  and  $\text{Gd@C}_{82}(\text{OH})_{22}$  suppress cell invasion and migration in pancreatic cancer.

In our previous study,  $\text{C}_{60}(\text{OH})_{22}$  and  $\text{Gd@C}_{82}(\text{OH})_{22}$  were found as reactive oxygen species (ROS) scavengers

in preventing the proliferation of cancer cells.<sup>41,43</sup> ROS stimulate angiogenesis and metastasis by increasing HIF-1 $\alpha$  under hypoxia.<sup>44,45</sup> Under normoxia, HIF-1 $\alpha$  exhibits a high level of expression in pancreatic cancer cells.<sup>19,46</sup> The level of ROS was reduced in Panc5.04 and Panc3.11 cells under normoxia after treatment with C<sub>60</sub>(OH)<sub>22</sub> or Gd@C<sub>82</sub>(OH)<sub>22</sub> (Figure 1b and Supporting Information Figure S1c). The results suggest that C<sub>60</sub>(OH)<sub>22</sub> and Gd@C<sub>82</sub>(OH)<sub>22</sub> suppress cell metastasis by reducing the level of ROS. HIF-1 $\alpha$  was undetectable in the majority of human tumors under normoxia.<sup>18,38</sup> However, consistent expression of HIF-1 $\alpha$  and a high level of spontaneous ROS were reported in pancreatic cancer cell lines under normoxia.<sup>18,47,48</sup> The level of HIF-1 $\alpha$  and ROS was reduced significantly after C<sub>60</sub>(OH)<sub>60</sub> or Gd@C<sub>82</sub>(OH)<sub>22</sub> treatment in Panc5.04 and Panc3.11 cells (Figure 1b,d and Supporting Information Figure S1d,f), which is similar to our recent reports.<sup>41,49–51</sup> Multiple studies support that the expression of HIF-1 $\alpha$  is inhibited by blocking class I/II HDACs with HDACIs in human cancers.<sup>38,39</sup> Trichostatin A (TSA),<sup>52</sup> FK228, butyrate, and LAQ82481 were found to suppress angiogenesis and to repress the expression of VEGF and MMP-2/9 in human cancer.<sup>53–56</sup> To further understand the mechanism of C<sub>60</sub>(OH)<sub>20</sub> and Gd@C<sub>82</sub>(OH)<sub>22</sub> in human pancreatic cancer, the expression of HDAC1 and HIF-1 $\alpha$  was detected before and after C<sub>60</sub>(OH)<sub>22</sub> or Gd@C<sub>82</sub>(OH)<sub>22</sub> treatment in Panc5.04 and Panc3.11 cells. The expression of HDAC1 and HIF-1 $\alpha$  was reduced noticeably after C<sub>60</sub>(OH)<sub>20</sub> or Gd@C<sub>82</sub>(OH)<sub>22</sub> treatment (Figure 1c,d and Supporting Information Figure S1e,f). In recent reports, intracellular ROS levels were suppressed by TSA, a HDAC inhibitor in both mice and humans.<sup>57,58</sup> Therefore, our results strongly suggest that C<sub>60</sub>(OH)<sub>22</sub> and Gd@C<sub>82</sub>(OH)<sub>22</sub> may serve as potential HDAC inhibitors in pancreatic cancer.

**Gd@C<sub>82</sub>(OH)<sub>22</sub> Nondestructively Interacts with HDAC1.** To understand the atomistic details of the *in vitro* experimental results, *in silico* molecular dynamics simulations were carried out to investigate the protein–nanoparticle interaction. Of special interest was how the two nanoparticles, Gd@C<sub>82</sub>(OH)<sub>22</sub> and C<sub>60</sub>(OH)<sub>22</sub>, affected possible association of HDAC1 with a co-repressor (e.g., MTA1) and/or co-regulator (e.g., D-myo-inositol-1,4,5,6-tetrakisphosphate (Ins(1,4,5,6)P4)) within the cancerous environment. For the simulations, each system consists of a HDAC1 surrounded by multiple Gd@C<sub>82</sub>(OH)<sub>22</sub> (or C<sub>60</sub>(OH)<sub>22</sub> as control) in explicit solvent without any initial contact between the molecules (Figure 2). For statistical analysis, five different >200 ns long trajectories were generated for each system in the isobaric and isothermal ensemble (*i.e.*, NPT ensemble in 1 atm and 310 K), resulting in over 2.2  $\mu$ s simulation time in the aggregate (see Methods and Supporting Information for more details).

Over the simulation time (*i.e.*, > 200 ns), HDAC1 keeps its native fold with all three metal binding sites intact (*i.e.*, one zinc-coordinated active site and two structural potassium binding sites) in all trajectories. Both the root mean square deviation (Supporting Information Figure S2) and root mean square fluctuation (Supporting Information Figure S3) of HDAC1 indicate that, except for the loop between residues G202 and D210, HDAC1 is quite rigid, even with frequent contact with the nanoparticles. For the flexible loop, some contacts were observed with Gd@C<sub>82</sub>(OH)<sub>22</sub> but rarely with C<sub>60</sub>(OH)<sub>22</sub>. Since this loop is located near one of the MTA1 binding domains (*i.e.*, ELM2-specific motif), it is possible that it might become stabilized once bound with MTA1.

Our simulations demonstrate that both fullerene derivatives hardly alter the tertiary structure of HDAC1 even locally. This is largely attributed to the multiple hydroxyl groups on the fullerene cages that result in better water solubility. Thus, Gd@C<sub>82</sub>(OH)<sub>22</sub> is not so hydrophobic as to deform the native structure of proteins, in contrast to bare carbon materials that cause large structure alterations.<sup>59,60</sup> However, Gd@C<sub>82</sub>(OH)<sub>22</sub> is not profoundly hydrophilic either,<sup>42</sup> which explains why these nanoparticles tend to cluster together and interact with proteins instead of being fully dissolved in water. Snapshots of one representative trajectory showing intensive interaction between multiple Gd@C<sub>82</sub>(OH)<sub>22</sub> with HDAC1 even with no obvious structural deformation can be seen in Figure 2d.

**Gd@C<sub>82</sub>(OH)<sub>22</sub> and C<sub>60</sub>(OH)<sub>22</sub> Have Different Binding Modes with HDAC1.** As shown in Figure 3, the site-specific contacts of HDAC1 with each fullerene derivative clearly distinguish binding modes. For instance, by comparing Figure 3b,e, it is readily seen that Gd@C<sub>82</sub>(OH)<sub>22</sub> prefers the N-terminal residues, whereas C<sub>60</sub>(OH)<sub>22</sub> favors the C-terminal ones. More explicitly, the projection of the contact sites onto the 3-D structure of HDAC1 (Figure 3a,d) indicates that the highly occupied sites by Gd@C<sub>82</sub>(OH)<sub>22</sub> coincide well with the MTA1 binding sites, which is not true in the case of C<sub>60</sub>(OH)<sub>22</sub>. This implies that Gd@C<sub>82</sub>(OH)<sub>22</sub> possibly inhibits HDAC1 by more indirectly interfering with the protein–protein association such as with co-repressor MTA1, so as to fail in recruiting HDAC1 properly. On the other hand, C<sub>60</sub>(OH)<sub>22</sub>, more in an indirect pathway, seems less effective than Gd@C<sub>82</sub>(OH)<sub>22</sub> in inhibiting HDAC1. As shown, the high-frequency contact sites of C<sub>60</sub>(OH)<sub>22</sub> have little overlap with MTA1 association domains. Of interest is the active site usually targeted by conventional HDAC inhibitors for histone tail deacetylation.<sup>7,13,14</sup> While we did observe some contacts between the active site and Gd@C<sub>82</sub>(OH)<sub>22</sub> (very rare with C<sub>60</sub>(OH)<sub>22</sub>), it is hard to propose that Gd@C<sub>82</sub>(OH)<sub>22</sub> inhibits HDAC1 dominantly by directly acting on this active site because a much larger contact area is predominantly populated at sites remote from it.

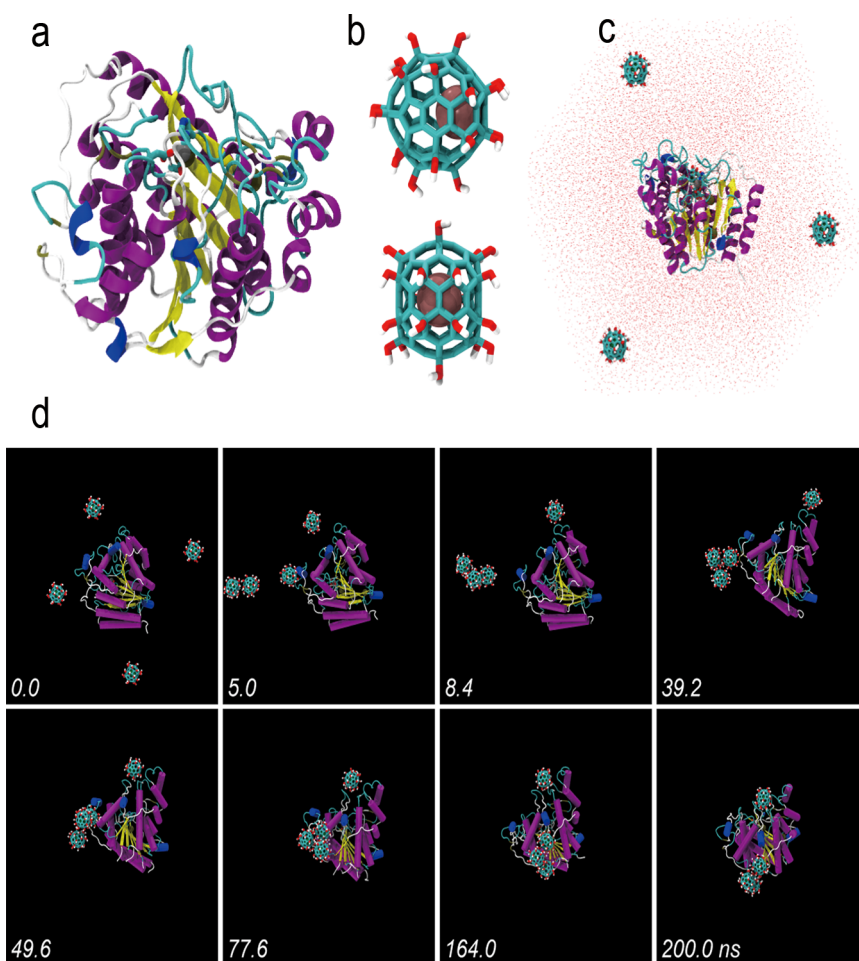


**Figure 2.** Molecular dynamics simulation with HDAC1 and Gd@C<sub>82</sub>(OH)<sub>22</sub>. (a) X-ray crystal structure of HDAC1. The zinc-coordinated active site is indicated with a ball (gray) coordinated with residues D176, H178, and D264, while the rest is colored depending on secondary structures (purple,  $\alpha$ -helix; blue,  $\beta_10$ -helix; yellow,  $\beta$ -sheet; cyan, turn; coil, white). (b) Molecular structure of Gd@C<sub>82</sub>(OH)<sub>22</sub>, where the Gd<sup>3+</sup> (green ball) ion is engaged in C<sub>82</sub>(OH)<sub>22</sub>. (c) Initial configuration of the molecular dynamics simulation. HDAC1 surrounded by four Gd@C<sub>82</sub>(OH)<sub>22</sub> is immersed in a 0.1 M NaCl TIP3P water solution. (d) Representative simulation trajectory, featured with a single and/or clustered contact at 8.4 and 39.2 ns, respectively, and further site search for thermodynamically stable bindings (49.6–200.0 ns) at co-repressor MTA1 binding sites.

**Gd@C<sub>82</sub>(OH)<sub>22</sub> Inhibits HDAC1 in Human Pancreatic Cancer Cells.** Histone acetylation alters chromatin structure and activates gene expression. HDAC1 suppresses gene expression by promoting histone deacetylation in the promoter region.<sup>61</sup> According to our computer simulations, Gd@C<sub>82</sub>(OH)<sub>22</sub> is more effective than C<sub>60</sub>(OH)<sub>22</sub> at binding with HDAC1. To validate the prediction results, we focused on the interaction of Gd@C<sub>82</sub>(OH)<sub>22</sub> with HDAC1 in pancreatic cancer cells. Acetylation of histone-H3 (H3K9, H3K14) and H4 (H4K5, H4K8, H4K16) was detected before and after Gd@C<sub>82</sub>(OH)<sub>22</sub> treatment in Panc5.04 and Panc3.11 cells. As shown in Supporting Information Figure S4, the level of acetylated histone-H3 and -H4 increased markedly after Gd@C<sub>82</sub>(OH)<sub>22</sub> treatment. The results suggest that Gd@C<sub>82</sub>(OH)<sub>22</sub> interacts with HDAC1 and inhibits its function. The expression of MTA1 and MMP-2/9 was reduced, and the expression of RECK increased noticeably after Gd@C<sub>82</sub>(OH)<sub>22</sub> treatment (Figure 1d, Figure 4a, Supporting Information Figures S1f and S8a). To further

validate that the expression of RECK was regulated by histone modification, the status of H3K9 acetylation in the RECK promoter region was examined by ChIP assay. The results suggest that histone H3K9 was apparently acetylated after Gd@C<sub>82</sub>(OH)<sub>22</sub> treatment in Panc5.04 (Figure 4b) and Panc3.11 cells (Supporting Information Figure S8b).

As reported before, the expression of RECK was inhibited by recruiting HDAC1 to its promoter region through MTA1 and HIF-1 $\alpha$ .<sup>7,62</sup> The 50% inhibitory concentration of Gd@C<sub>82</sub>(OH)<sub>22</sub> on the interaction of HDAC1 and MTA1 is 50  $\mu$ M for 6 h, and the expression of HDAC1 and MTA1 was not inhibited by treatment with Gd@C<sub>82</sub>(OH)<sub>22</sub> at 50  $\mu$ M for 2 h. Therefore, the interaction of MTA1, HDAC1, and HIF-1 $\alpha$  was analyzed by immunofluorescence and CoIP assay before and after 50  $\mu$ M Gd@C<sub>82</sub>(OH)<sub>22</sub> treatment for 2 h. The complex bands were strong before Gd@C<sub>82</sub>(OH)<sub>22</sub> treatment. The bands became faint after Gd@C<sub>82</sub>(OH)<sub>22</sub> treatment in Panc5.04 and Panc3.11 cells (Figure 4d and

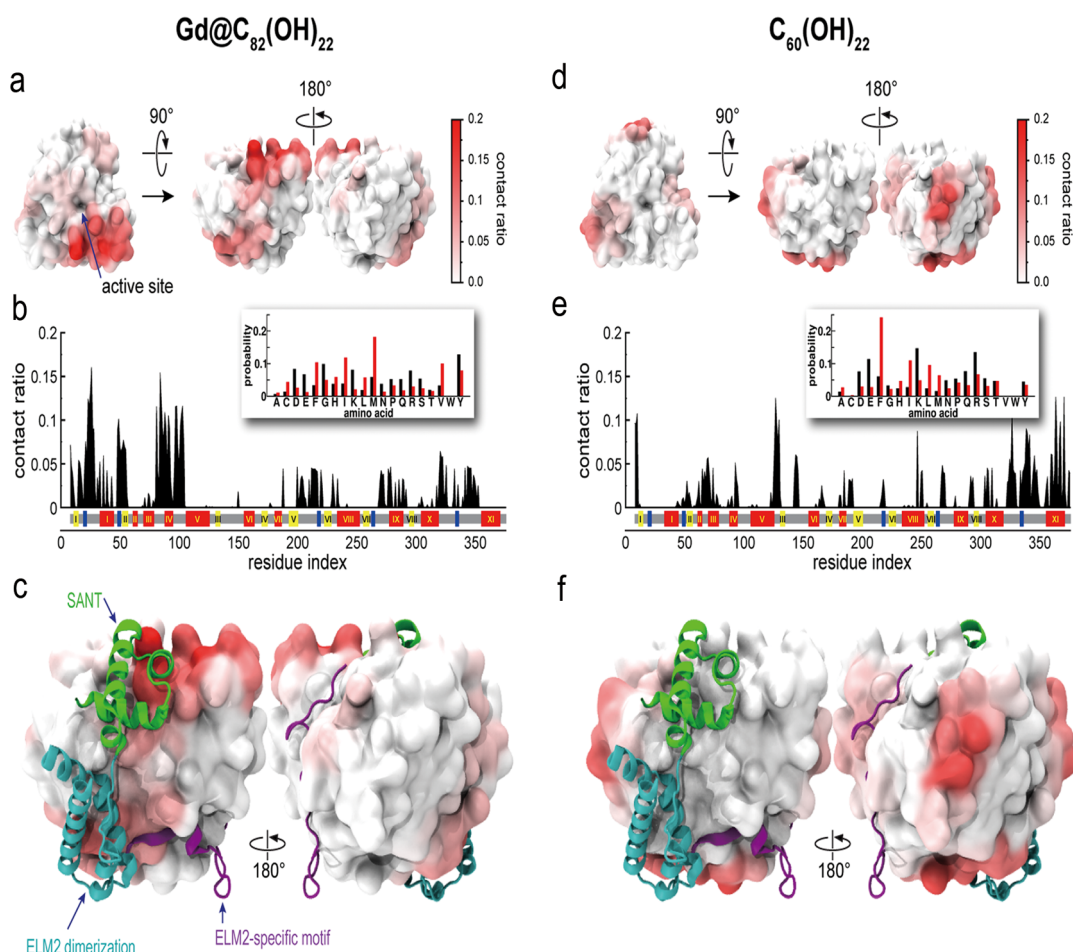


**Figure 3.** Site-specific contacts on HDAC1 by  $\text{Gd}@\text{C}_{82}(\text{OH})_{22}$  (left column) and  $\text{C}_{60}(\text{OH})_{22}$  (right column). (a,d) Favorable contact sites projected on the surface of HDAC1, where the binding sites seem complementary between fullerene derivatives. (b,e) Residue-specific contact ratios along the sequence of HDAC1 and amino-acid-specific contact probabilities (inset; black bars, probabilities over amino acid types, and red bars, probabilities normalized by the surface amino acid density with an exposure cutoff of SASA > 40%).  $\text{Gd}@\text{C}_{82}(\text{OH})_{22}$  has a favorable interaction in groups, especially at the N-terminal region of HDAC1, whereas  $\text{C}_{60}(\text{OH})_{22}$  has a much choppier contact all over the sequence. (c,f) HDAC1 contacts overlaid with MTA1.  $\text{Gd}@\text{C}_{82}(\text{OH})_{22}$  intensively interacts at HDAC1 sites, where MTA1 binds and  $\text{C}_{60}(\text{OH})_{22}$  contacts at sites remote from MTA1 binding sites.

Supporting Information Figure S8d). These results further suggest that MTA1, HDAC1, and HIF-1 $\alpha$  formed a complex and that HDAC1 was recruited by MTA1 and HIF-1 $\alpha$  in the RECK promoter region.  $\text{Gd}@\text{C}_{82}(\text{OH})_{22}$  activates RECK expression by inhibiting the interaction of HDAC1, MTA1, and HIF-1 $\alpha$  in the promoter region. The number of invasive and migration cells was reduced by knocking down HDAC1 in Panc5.04 and Panc3.11 cells (Supporting Information Figure S13a,b). The expression of RECK was increased, and the expression of MMP-2/9 was reduced after knockdown of HDAC1 (Supporting Information Figure S5). The result further indicates that  $\text{Gd}@\text{C}_{82}(\text{OH})_{22}$  induces RECK expression by inhibiting HDAC1 expression and recruiting HDAC1 to the RECK promoter region.

MMP-2 and MMP-9 were reported to be regulated by RECK. To further validate that MMP-2 and MMP-9 are down-regulated by RECK under  $\text{Gd}@\text{C}_{82}(\text{OH})_{22}$  treatment, siRNA knockdown technique was employed. The expression of RECK was induced, and MMP-2/9

expression was suppressed by  $\text{Gd}@\text{C}_{82}(\text{OH})_{22}$  treatment at 50  $\mu\text{M}$  for 24 h; then RECK was knocked down by siRNA. The number of invasive cells increased significantly in the siRNA knockdown group compared with the scrambled siRNA treated group after treatment ( $P < 0.05$ ). MMP-2/9 expression was inhibited after  $\text{Gd}@\text{C}_{82}(\text{OH})_{22}$  treatment for 24 h. Re-expression of MMP-2/9 was induced by knocking down RECK (Supporting Information Figure S13c,d). The results above suggest that  $\text{Gd}@\text{C}_{82}(\text{OH})_{22}$  suppresses pancreatic cancer invasion and was caused by down-regulation of MMP-2/9 through inhibition of HDAC1-induced up-regulation of RECK.

**$\text{Gd}@\text{C}_{82}(\text{OH})_{22}$  Inhibits HDAC1 Activity by Effectively Interfering with Co-repressor MTA1 Association.** As a histone deacetylation enzyme, HDAC1 needs to conjugate with a co-repressor, such as MTA1, to recognize the targeting location in chromatin and to align in the correct orientation according to the substrates at the histone tail. Thus, a stable complex of HDAC1 with a cognate

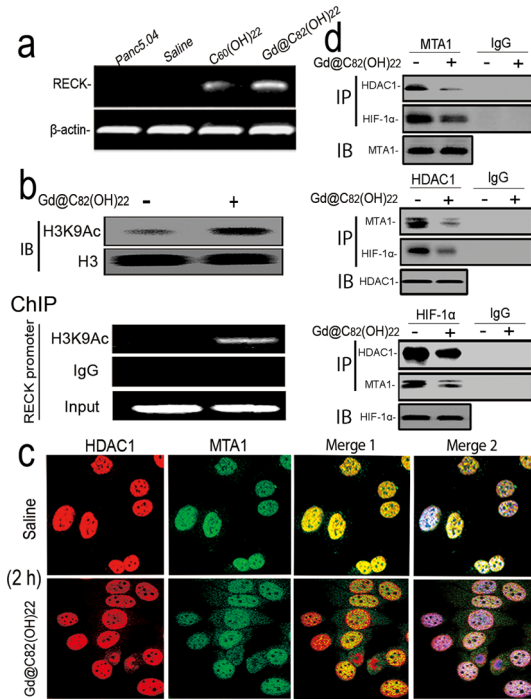


**Figure 4. Mechanism of  $C_{60}(OH)_{22}$  and  $Gd@C_{82}(OH)_{22}$  on the regulation of RECK expression at the concentration of  $50\ \mu M$  for 24 h and the effect of  $Gd@C_{82}(OH)_{22}$  on the interaction of HDAC1 with MTA1 at the concentration of  $50\ \mu M$  for 2 h in Panc5.04 cells. (a) Reverse-transcriptase polymerase chain reaction results show the effect of  $C_{60}(OH)_{22}$  and  $Gd@C_{82}(OH)_{22}$  on the expression of RECK at the concentration of  $50\ \mu M$  for 24 h in Panc5.04 cells.  $Gd@C_{82}(OH)_{22}$  is more effective than  $C_{60}(OH)_{22}$ . (b) Western blot and ChIP assay results show  $Gd@C_{82}(OH)_{22}$  activated H3K9Ac acetylation in the RECK promoter region at  $50\ \mu M$  in 24 h (IgG: negative control with nonspecific antibody). (c) In order to prevent the degradation of HDAC1 and MTA1 before finishing detection of the interaction of MTA1 and HDAC1, Panc5.04 cells were treated with  $Gd@C_{82}(OH)_{22}$  for only 2 h at the concentration of  $50\ \mu M$ . Immunofluorescence assay shows that the interaction of MTA1 and HDAC1 was inhibited by  $Gd@C_{82}(OH)_{22}$  in Panc5.04 cells (red, HDAC1 coupled with tetramethylrhodamine; green, MTA1 coupled with FITC). Merge 1: Interaction of HDAC1 and MTA1. Merge 2: Fusion with Merge 1 and DAPI (nuclei, blue). (d) CoIP results show the interaction of HDAC1, HIF-1α, and MTA1. (+)  $Gd@C_{82}(OH)_{22}$  treatment, (-) no  $Gd@C_{82}(OH)_{22}$  treatment.**

co-repressor is an important prerequisite for chromatin condensation following transcriptional repression. The MTA1 binding on HDAC1 has been characterized by an extensive interaction with the three domains of MTA1, such as SANT (residues 283MTA1–335MTA1), ELM2 dimerization (residues 199MTA1–282MTA1), and ELM2-specific motif (residues 162MTA1–198MTA1), along with the carboxy to amino termini of MTA1.

More specifically, we constructed potential of mean forces (PMFs) on the surface of HDAC1 based on the residue-specific contact probability (Figure 5). As shown in the contact analysis, PMF also shows that  $Gd@C_{82}(OH)_{22}$  has a favorable interaction with HDAC1 along MTA1 binding sites, especially at SANT and ELM2 dimerization domains. The energetics behind the binding pattern could be rationalized by analyzing

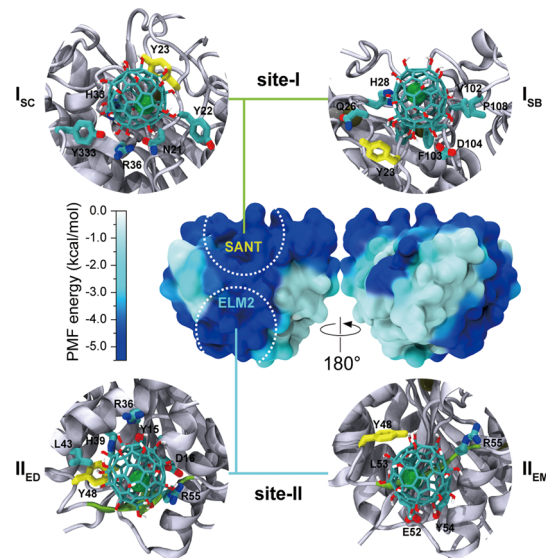


**Figure 5. Potential of mean force and representative binding modes.** The binding PMF projected on the HDAC1 surface clarifies that  $Gd@C_{82}(OH)_{22}$  has thermodynamically stable interactions at two sites that are very important to MTA1 association, as indicated with site-I and site-II. The PMF has been calculated by  $w(r) = -RT \ln p(r)$ , where  $p(r)$  is the contact probability at a residue  $r$  by nanoparticles. In each, two representative binding modes are proposed, each having stable interactions with surface residues. At site-I,  $Gd@C_{82}(OH)_{22}$  may interfere with the MTA1–SANT domain binding as well as the co-regulator  $Ins(1,4,5,6)P_4$ . At site-II,  $Gd@C_{82}(OH)_{22}$  seems to effectively block the MTA1–ELM2 dimerization domain especially in mode II<sub>ED</sub>, as well as the ELM2-specific motif in mode II<sub>EM</sub> by interfering with anti-parallel β-strand packing against HDAC1 (as marked with a green ribbon).

surface electrostatics on HDAC1 (Supporting Information Figure S6). The isoelectric surface shows that MTA1 interacts on HDAC1 in a large striped area, composed of neutral or positively charged residues. Given that the negative charge on the fullerol cage is induced by the encaged  $Gd^{3+}$  (*i.e.*,  $Gd^{3+}@[C_{82}(OH)_{22}]^{3-}$ ),  $Gd@C_{82}(OH)_{22}$  would be more likely to make its first contacts with positively charged residues by virtue of the long-ranged electrostatic interactions. Once near the protein surface, however,  $Gd@C_{82}(OH)_{22}$  can diversify the interacting residues by using relatively short-ranged hydrophobic, aromatic, and hydrogen bonding interactions in addition to the electrostatic interaction. This enables  $Gd@C_{82}(OH)_{22}$  to interact even with negatively charged amino acids like Asp and Glu.

Based on the PMF analysis, two energetically favorable binding sites on HDAC1 for  $Gd@C_{82}(OH)_{22}$  are identified, which we marked as site-I and site-II. Site-I directly corresponds to the binding site for the SANT domain of MTA1, which is critical in recruiting class I HDAC with the aid of co-regulator  $Ins(1,4,5,6)P_4$ .<sup>63</sup> For site-II, it coincides with the binding sites for the amino end of the ELM2 dimerization domain and the carboxy end of the ELM2-specific motif of MTA1.

For site-I, two representative binding modes are found to associate with this location from the simulations,

namely, ISC and ISB. In mode ISC, Gd@C<sub>82</sub>(OH)<sub>22</sub> interacts with residues that are known to play an important role at the center of the interface between MTA1–SANT and HDAC1, including N21, Y22, Y23, H33, R36, and Y333. For example, H33 and Y333 have been shown to provide a stage for stable aromatic interaction with Y327MTA1 and Y328MTA1 of the SANT domain, which is crucial in coordinating Ins(1,4,5,6)P<sub>4</sub> to make HDAC1 active.<sup>63</sup> On the other hand, during mode ISB, Gd@C<sub>82</sub>(OH)<sub>22</sub> interacts with residues located along the border of the binding sites of the SANT domain, which include residues Y23, Y24, Q26, H28, V102, F103, D104, and P108. Although Gd@C<sub>82</sub>(OH)<sub>22</sub> might not effectively inhibit the SANT binding in this mode, it could interfere in important interactions, such as the hydrophobic interaction made by Y23 and the hydrogen bonding network between Q26, K305MTA1, and D306MTA1.

Similar to site-I, two representative binding modes are also observed at site-II, which we named modes II<sub>ED</sub> and II<sub>EM</sub>. However, unlike site-I, Gd@C<sub>82</sub>(OH)<sub>22</sub> interacts with HDAC1 in the middle of the protein–protein interface in these two modes. For example, in mode II<sub>ED</sub>, Gd@C<sub>82</sub>(OH)<sub>22</sub> directly interacts with key residues that are important for the MTA1–ELM2 dimerization domain binding, including Y15, D16, R36, H39, L43, Y48 and R49. These aromatic and hydrophobic residues are all involved in hydrophobic contacts with residues of MTA1, and R49 forms stable electrostatic interactions with D207MTA1 and D111MTA1. Meanwhile, mode II<sub>EM</sub> shows that Gd@C<sub>82</sub>(OH)<sub>22</sub> has a strong contact with E52, L53, Y54, and R55 of β-strand site-II, which correspond to the binding site for the C-terminal region of the ELM2-specific motif of MTA1. While a majority of ELM2-specific motifs lack secondary structure even bound with HDAC1, the C-terminal end of this domain forms a short β-strand (residues L194MTA1 to W199MTA1) packed antiparallel against a β-strand site-II (*i.e.*, G52 to P56) of HDAC1. Therefore, the intensive interaction of Gd@C<sub>82</sub>(OH)<sub>22</sub> at the β-strand site-II possibly interferes with antiparallel β-strand formation between HDAC1 and MTA1, again resulting in attenuated HDAC1 recruitment.

Taken together, our simulations showed that both Gd@C<sub>82</sub>(OH)<sub>22</sub> and C<sub>60</sub>(OH)<sub>22</sub> have drastically different binding modes on HDAC1. Although a direct blockage on the active site was not found as a predominant pathway for both nanoparticles, strikingly, Gd@C<sub>82</sub>(OH)<sub>22</sub> has a thermodynamically stable interaction along the HDAC1 surface that is critical for the co-repressor MTA1 binding domains, including SANT, ELM2 dimerization, and the C-terminal end of the ELM2-specific motif. To the contrary, C<sub>60</sub>(OH)<sub>22</sub> contacted with HDAC1 at less critical and seemingly complementary sites from those of Gd@C<sub>82</sub>(OH)<sub>22</sub>. This strongly suggests a potential inhibitory mechanism of Gd@C<sub>82</sub>(OH)<sub>22</sub> on HDAC1–Gd@C<sub>82</sub>(OH)<sub>22</sub>, acting as an

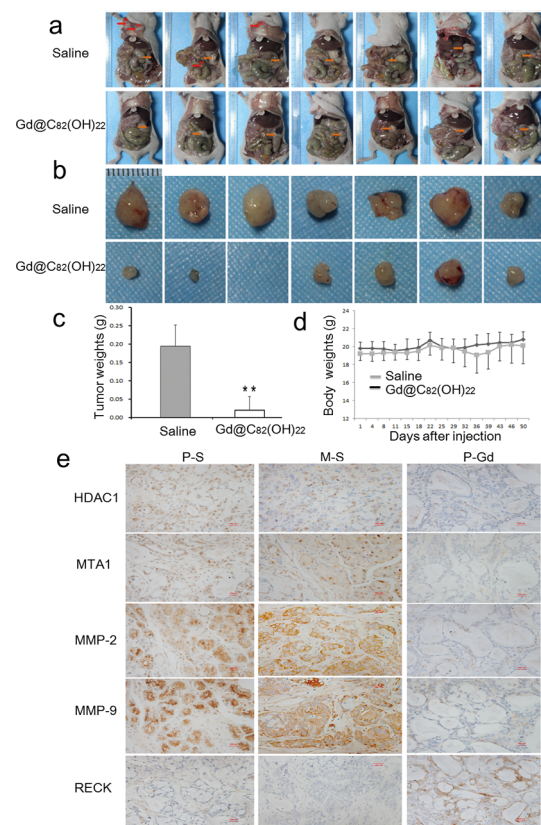


**Figure 6.** Gd@C<sub>82</sub>(OH)<sub>22</sub> suppresses tumor growth and metastasis in Panc5.04 cell xenograft mice. (a) Primary and metastatic tumors in Panc5.04 cell xenograft mice. Distant metastasis occurred in 3 of 7 saline-treated mice groups, and no distant metastasis was observed in the Gd@C<sub>82</sub>(OH)<sub>22</sub>-treated group. (b) Volume of Panc5.04 primary tumor xenografts in the Gd@C<sub>82</sub>(OH)<sub>22</sub>-treated group was apparently smaller than that in the control group. (c) Tumor weight was measured at the time point of 50 days. The reduction of tumor mass was observed in the Gd@C<sub>82</sub>(OH)<sub>22</sub>-treated group (\*\**P* < 0.01). (d) There is no difference in the variation of body weight change between Gd@C<sub>82</sub>(OH)<sub>22</sub>-treated and saline-treated groups. (e) IHC staining was performed to detect the expression of metastasis-related factors in primary tumors and metastatic tumors (P-S, primary tumors in saline group; M-S, metastatic tumor sites in saline group; P-Gd, primary tumors in Gd@C<sub>82</sub>(OH)<sub>22</sub>-treated group) including HDAC1, MTA1, MMP-2, MMP-9, and antimetastatic factor, RECK. Down-regulation of HDAC1, MTA1, and MMP-2/9 was observed, and up-regulation of RECK was detected in the Gd@C<sub>82</sub>(OH)<sub>22</sub>-treated group.

effective inhibitor for protein–protein association between HDAC1 and MTA1 rather than an inhibitor to directly block a ligand binding at the active site of HDAC1.

The interaction of HDAC1 and MTA1 is inhibited by Gd@C<sub>82</sub>(OH)<sub>22</sub> according to our molecular simulations. To validate this prediction, the CoIP technique was employed. First, we analyzed the time course and the dosage of Gd@C<sub>82</sub>(OH)<sub>22</sub> on HDAC1 and MTA1 expression inhibition in Panc5.04 cells (Supporting Information Figure S7). No HDAC1 expression and very weak expression of MTA1 were found in Panc5.04 and Panc3.11 cells after Gd@C<sub>82</sub>(OH)<sub>22</sub> treatment at 50 μM

for 24 h (Figure 1d and Supporting Information Figure S1f). The inhibiting effect on the expression of HDAC1 and MTA1 was enhanced with the increased exposure time. As the expression of HDAC1 and MTA1 was not inhibited by treatment with Gd@C<sub>82</sub>(OH)<sub>22</sub> at 50 μM for 2 h, we evaluated the effect of Gd@C<sub>82</sub>(OH)<sub>22</sub> on the interaction of HDAC1 and MTA1 under this condition (Figure 4). As shown in Figure 4 and Supporting Information Figure S8, the interaction of HDAC1 and MTA1 was suppressed by addition of Gd@C<sub>82</sub>(OH)<sub>22</sub> to Panc5.04 and Panc3.11 cells. The inhibition of Gd@C<sub>82</sub>(OH)<sub>22</sub> on the interaction of HDAC1 and MTA1 was further validated by immunofluorescence (Figure 4c and Supporting Information Figure S8c), confirming the predictions from our computer modeling. The results above suggest that Gd@C<sub>82</sub>(OH)<sub>22</sub> may inhibit the interaction of HDAC1 and MTA1, as well as regulation of HDAC1 expression. To validate that Gd@C<sub>82</sub>(OH)<sub>22</sub> is directly bound to HDAC1, precipitation of HDAC1 and MTA1 was performed following the treatment of Gd@C<sub>82</sub>(OH)<sub>22</sub> in Panc5.04 and Panc3.11 cells. As shown in Supporting Information Figure S14, Gd@C<sub>82</sub>(OH)<sub>22</sub> was bound to HDAC1 and MTA1 but not IgG (negative control). The results strongly demonstrate that Gd@C<sub>82</sub>(OH)<sub>22</sub> is directly bound to HDAC1.

**Gd@C<sub>82</sub>(OH)<sub>22</sub> Suppresses Pancreatic Cancer Metastasis in Panc5.04 Xenograft Mice.** To validate the effect of Gd@C<sub>82</sub>(OH)<sub>22</sub> on pancreatic cancer metastasis, a primary pancreatic tumor xenograft mouse model was established from resection specimens of Panc5.04 tumors. Distant metastasis occurred in 3 of 7 saline-treated mice, and no distant metastasis was observed in the Gd@C<sub>82</sub>(OH)<sub>22</sub>-treated group (Figure 6a). No distant metastasis was found in both Gd@C<sub>82</sub>(OH)<sub>22</sub>-treated

and saline-treated Panc3.11 primary pancreatic tumor xenograft mice (Supporting Information Figure S12). The volume and weight of Panc5.04 cell and Panc3.11 cell primary tumor xenografts in the Gd@C<sub>82</sub>(OH)<sub>22</sub>-treated group were significantly smaller than those in the control group at the time point of 50 days (Figure 6b,c and Supporting Information Figure S12, all  $P < 0.01$ ). As shown in Figure 6d, the body weight showed no significant difference between the Gd@C<sub>82</sub>(OH)<sub>22</sub>-treated group and saline-treated group. Immunohistochemical (IHC) staining was performed to detect the expression of metastasis-related genes in primary tumors and metastatic tumors, including HDAC1, MTA1, MMP-2, MMP-9, and RECK. Down-regulation of HDAC1, MTA1, and MMP-2/9 was observed, and up-regulation of RECK was detected in the Gd@C<sub>82</sub>(OH)<sub>22</sub>-treated group (Figure 6e). These results further suggest that Gd@C<sub>82</sub>(OH)<sub>22</sub> suppresses pancreatic cancer metastasis by inhibiting HDAC1 expression in Panc5.04 cell xenograft mice.

## CONCLUSIONS

In summary, Gd@C<sub>82</sub>(OH)<sub>22</sub>, as a potential HDAC1 inhibitor, suppresses pancreatic cancer cell invasion and migration. Gd@C<sub>82</sub>(OH)<sub>22</sub> activates RECK expression by inhibiting the interaction of HDAC1, MTA1, and HIF-1α in the promoter region. The interaction of HDAC1 and MTA1 was inhibited by Gd@C<sub>82</sub>(OH)<sub>22</sub> according to both our computer modeling and experimental validation, which explains the suppression of MMP-2/9 expression and the downstream genes of HDAC1 and MTA1 interaction, and thus the metastasis of pancreatic cancer was inhibited by Gd@C<sub>82</sub>(OH)<sub>22</sub>.

## METHODS

**Cell Lines and Cell Culture.** C<sub>60</sub>(OH)<sub>22</sub> and Gd@C<sub>82</sub>(OH)<sub>22</sub> were dissolved in saline as stock solution at the final concentration of 2 mM. Panc5.04 and Panc3.11 cell lines were obtained from the American Type Culture Collection (Manassas, VA, USA) and cultured in RPMI-1640 with 10% fetal bovine serum (complete medium, Life Technology, Grand Island, USA).

**Transwell Migration Assay.** The effect of C<sub>60</sub>(OH)<sub>22</sub> and Gd@C<sub>82</sub>(OH)<sub>22</sub> on pancreatic cancer cell migration was detected by using the COSTAR transwell (Corning Incorporated, MA, USA). Panc5.04 and Panc3.11 cells were harvested and suspended in the serum-free medium. Cell suspensions were then placed into the upper well at a concentration of  $2 \times 10^4$  cells/200 μL, while the complete medium with 10% fetal bovine serum was placed into the lower well (500 μL). The chamber was incubated for 18 h. The cells still on the top surface were scraped gently and washed out with phosphate-buffered saline three times. The cells migrated to the lower surface of the membrane and were stained with crystal violet and counted in three independent high-power fields (200×).

**Cell Invasion Assay.** Panc5.04 and Panc3.11 cells ( $2 \times 10^4$ ) were suspended in 200 μL of serum-free medium and loaded onto the upper compartment of an invasion chamber containing a polycarbonate membrane with an 8 μm pore size, which was coated with a layer of extracellular matrix (ECM; Matrigel).

After 24 h of C<sub>60</sub>(OH)<sub>22</sub> and Gd@C<sub>82</sub>(OH)<sub>22</sub> treatment, the invasive cells migrated through the ECM layer to the complete medium in the lower compartment and were stained with crystal violet, and the number of invaded cells was counted in three independent high-power fields (200×).

**ROS Activity Detection.** The ROS production within the cells was measured by 2',7'-dichlorodihydrofluorescein diacetate according to the manufacturer's instruction (DCFDA; Beyotime Ltd., Haimen, Jiangsu Province, China), and the O<sub>2</sub><sup>•-</sup> production was analyzed by flow cytometry using dihydroethidium (DHE, Invitrogen, Carlsbad, CA, USA) fluorescent probes. Cells ( $1 \times 10^6$ ) were incubated with the fluorescent probes (5 μM) for 1 h at 37 °C, and the cells were washed and resuspended in phosphate-buffered saline and analyzed under DCF (494/519 nm) and DHE fluorescence (535/617 nm) using FACS Calibur (Becton-Dickinson, Rutherford, NJ). The median fluorescence intensity was quantitated by CellQuest software (Becton-Dickinson) analysis of the recorded histograms.

**siRNA Knockdown Assay.** The siRNA knockdown assay was performed according to the manufacturer's instructions. The sequences of siRNA are listed in Supporting Information Table S1 (Gene Pharma Co, Shanghai, China).

**Western Blot.** Antibodies were diluted according to manufacturer's instruction. Primary antibodies are as follows: HDAC1 (Beyotime Ltd., Haimen, China); HIF-1α, MMP-2, and MMP-9 (Abcam, Cambridge, UK); RECK (Abgent, San Diego, CA, USA),

MTA1 (CST, USA);  $\beta$ -actin (Sigma-Aldrich, St. Louis, MO, USA); total H3, H4, and acetylated H3K9, H3K14, H4K5, H4K8, and H4K16 (Abcam, Cambridge, UK).

**Immunofluorescence.** For imaging analysis for Panc5.04 and Panc3.11 cells treated by Gd@C<sub>82</sub>(OH)<sub>22</sub> or saline, the cells were stained with 4,6-diamidino-2-phenylindole (DAPI, Sigma, St. Louis, MO), and MTA1 antibody was coupled with FITC-labeled secondary antibody (494 nm ex/em 520 nm, color, green, Invitrogen, Life Technologies, Grand Island, USA); HDAC1 was indirectly coupled with tetramethylrhodamine-labeled secondary antibody (550 nm ex/em 620 nm, red color, Invitrogen) and was used for confocal analysis (Leica DM 4000 M fitted with polarizer, GE). Images were acquired and analyzed by the LAS suite 3.0 software.

**ChIP Assay (Chromatin Immunoprecipitation).** The histone acetylation status of the RECK promoter was examined using the chromatin immunoprecipitation assay. An antibody specific for acetylated histone H3 was used to immunoprecipitate formaldehyde cross-linked, sonicated chromatin from Gd@C<sub>82</sub>(OH)<sub>22</sub>-treated and untreated cells. Semiquantitative polymerase chain reaction (PCR) was applied to detect the fragment of the RECK promoter region in the complex ( $-130$  site to  $+45$  site; primers are listed in Supporting Information Table S1). Briefly, pancreatic carcinoma cells were fixed, and cell lysates were sonicated on ice. The lysates were treated with anti-Ach3K9 antibody (Abcam, Cambridge, UK) overnight at  $4^{\circ}\text{C}$ . Immune complexes were collected on a salmon sperm DNA/protein A/G agarose slurry and were then extracted from the beads with 1% SDS and 0.1 M NaHCO<sub>3</sub>. The DNA was recovered and subjected to PCR amplification.

**Co-immunoprecipitation Assay (CoIP).** Cell lysates were obtained from Gd@C<sub>82</sub>(OH)<sub>22</sub>-treated and untreated cells, and the antibodies were employed to probe the specific protein. IgG was used as the control.

**Knockdown of RECK by siRNA after Gd@C<sub>82</sub>(OH)<sub>22</sub> Treatment for 48 h in Panc5.04 and Panc3.11 Cells.** The expression of RECK was induced by Gd@C<sub>82</sub>(OH)<sub>22</sub> treatment at 50  $\mu\text{M}$  for 24 h. Then siRNA knockdown was performed. Two specific RECK siRNAs were used, and the scrambled siRNA was set as the negative control. After successful transfection of siRNA in Panc5.04 and Panc3.11 pancreatic cancer cells, the expression of RECK, MMP-2, and MMP-9 was determined by Western blot.

**Establishment of Primary Pancreatic Cancer Mice Model.** Five week old female athymic nude mice (BALB/c, Vitalriver, Ltd., China) were used to establish the primary pancreatic cancer model. The procedure was approved by the Institutional Animal Care and Use Committee of the PLA General Hospital. In addition, experiments were conducted according to the "Guidelines for the Welfare of Animals in Experimental Neoplasia" published by the Coordinating Committee on Cancer Research. The tumorigenicity of Panc5.04 or Panc3.11 cells was first evaluated in subcutaneous pancreatic cancer models. Cells ( $1 \times 10^6$ ) were injected into the subcutis (right flank) of nude mice ( $n = 3$ ). Tumor diameters were measured twice a week, and tumor volumes were determined by using the formula width<sup>2</sup>  $\times$  length  $\times$  0.5. Subcutaneous tumors were excised until the tumor diameter reached 10 mm. Then the tumors were cut to 1 mm<sup>3</sup> pieces and incubated into the pancreatic tail ( $n = 14$ ). Seven mice were injected with Gd@C<sub>82</sub>(OH)<sub>22</sub> by intraperitoneal administration (1  $\mu\text{mol}/\text{kg}/\text{day}$ , 100  $\mu\text{L}$ ). Another seven mice were administered saline (100  $\mu\text{L}$ ). Mice were sacrificed at the time point of 50 days; tumors were excised and weighed, and the distant metastasis was checked. Tumors were paraffin-embedded for IHC analysis. The expressions of HDAC1, MTA1, MMP-2, and MMP-9 were stained with IHC.

**Immunoprecipitation and Nuclear Extract Preparation.** Nuclei were isolated for Panc5.04 or Panc3.11 cells treated with saline (control) or Gd@C<sub>82</sub>(OH)<sub>22</sub> (50  $\mu\text{M}$ , 2 h), following the protocol instructions (Appligen Technologies Inc., Beijing, China) and incubated with HDAC1 or MTA1 antibody or IgG (negative control). Immunoprecipitates were washed six times to avoid the background. Concentrations of trace element Gd were determined with an inductively coupled plasma mass spectrometer (ICP-MS) (Thermo Elemental X7 series, UK) in standard mode. Gd amount was detected by ICP-MS assay in our previous

and other studies.<sup>64–67</sup> The experiment was repeated three times; \*\* indicates statistically significant differences ( $P < 0.01$ ).

**Statistical Analysis.** The results are represented as mean  $\pm$  standard deviation. A  $P$  value  $<0.05$  was considered to be significant. All statistical tests were two sided.

**Conflict of Interest:** The authors declare no competing financial interest.

**Acknowledgment.** This work was financially supported by grants from the National Basic Research Program (973 Program Nos. 2012CB934002, 2010CB912802, and 2011CB933400), National High Tech R&D Program (863 Program Nos. SS2012AA02A209, SS2012AA020821, and SS2012AA02A203), National Key Scientific Instrument Special Program of China (Grant 2011YQ03013405), the Major Equipment Program (2011YQ030134), and the National Science Foundation of China (Grants 81121004, 81071953, 81161120432, 1205166, 11435002, and 21320102003).

**Supporting Information Available:** Figures S1–S15, Table S1, including the primer sequences used. The Supporting Information is available free of charge on the ACS Publications website at DOI: 10.1021/nn506782f.

## REFERENCES AND NOTES

- Siegel, R.; Ma, J.; Zou, Z.; Jemal, A. *Cancer Statistics, 2014. CA-Cancer J. Clin.* **2014**, *64*, 9–29.
- Yadav, D.; Lowenfels, A. B. *The Epidemiology of Pancreatitis and Pancreatic Cancer. Gastroenterology* **2013**, *144*, 1252–1261.
- Bosetti, C.; Bertuccio, P.; Negri, E.; La Vecchia, C.; Zeegers, M. P.; Boffetta, P. *Pancreatic Cancer: Overview of Descriptive Epidemiology. Mol. Carcinog.* **2012**, *51*, 3–13.
- Neoptolemos, J. P.; Stocken, D. D.; Friess, H.; Bassi, C.; Dunn, J. A.; Hickey, H.; Beger, H.; Fernandez-Cruz, L.; Dervenis, C.; Lacaine, F.; et al. *A Randomized Trial of Chemoradiotherapy and Chemotherapy after Resection of Pancreatic Cancer. N. Engl. J. Med.* **2004**, *350*, 1200–1210.
- Yoo, Y. G.; Na, T. Y.; Seo, H. W.; Seong, J. K.; Park, C. K.; Shin, Y. K.; Lee, M. O. *Hepatitis B Virus X Protein Induces the Expression of MTA1 and HDAC1, Which Enhances Hypoxia Signaling in Hepatocellular Carcinoma Cells. Oncogene* **2008**, *27*, 3405–3413.
- Toh, Y.; Kuninaka, S.; Endo, K.; Oshiro, T.; Ikeda, Y.; Nakashima, H.; Baba, H.; Kohnoe, S.; Okamura, T.; Nicolson, G. L.; et al. *Molecular Analysis of a Candidate Metastasis-Associated Gene, MTA1: Possible Interaction with Histone Deacetylase 1. J. Exp Clin. Cancer Res.* **2000**, *19*, 105–111.
- Jeon, H. W.; Lee, Y. M. *Inhibition of Histone Deacetylase Attenuates Hypoxia-Induced Migration and Invasion of Cancer Cells via the Restoration of RECK Expression. Mol. Cancer Ther.* **2010**, *9*, 1361–1370.
- Oh, J.; Takahashi, R.; Kondo, S.; Mizoguchi, A.; Adachi, E.; Sasahara, R. M.; Nishimura, S.; Imamura, Y.; Kitayama, H.; Alexander, D. B.; et al. *The Membrane-Anchored MMP Inhibitor RECK Is a Key Regulator of Extracellular Matrix Integrity and Angiogenesis. Cell* **2001**, *107*, 789–800.
- Masui, T.; Doi, R.; Koshiba, T.; Fujimoto, K.; Tsuji, S.; Nakajima, S.; Koizumi, M.; Toyoda, E.; Tulachan, S.; Ito, D.; et al. *RECK Expression in Pancreatic Cancer: Its Correlation with Lower Invasiveness and Better Prognosis. Clin. Cancer Res.* **2003**, *9*, 1779–1784.
- Noda, M.; Oh, J.; Takahashi, R.; Kondo, S.; Kitayama, H.; Takahashi, C. *RECK: A Novel Suppressor of Malignancy Linking Oncogenic Signaling to Extracellular Matrix Remodeling. Cancer Metastasis Rev.* **2003**, *22*, 167–175.
- Takagi, S.; Simizu, S.; Osada, H. *RECK Negatively Regulates Matrix Metalloproteinase-9 Transcription. Cancer Res.* **2009**, *69*, 1502–1508.
- Silveira Correa, T. C.; Massaro, R. R.; Brohem, C. A.; Taboga, S. R.; Lamers, M. L.; Santos, M. F.; Maria-Engler, S. S. *RECK-Mediated Inhibition of Glioma Migration and Invasion. J. Cell. Biochem.* **2010**, *110*, 52–61.
- Liu, L. T.; Chang, H. C.; Chiang, L. C.; Hung, W. C. *Histone Deacetylase Inhibitor Up-Regulates RECK To Inhibit*

- MMP-2 Activation and Cancer Cell Invasion. *Cancer Res.* **2003**, *63*, 3069–3072.
14. Chang, H. C.; Liu, L. T.; Hung, W. C. Involvement of Histone Deacetylation in Ras-Induced Down-Regulation of the Metastasis Suppressor RECK. *Cell Signal* **2004**, *16*, 675–679.
  15. Vadlapatla, R. K.; Vadlapudi, A. D.; Mitra, A. K. Hypoxia-Inducible Factor-1 (HIF-1): A Potential Target for Intervention in Ocular Neovascular Diseases. *Curr. Drug Targets* **2013**, *14*, 919–935.
  16. Yang, M. H.; Wu, K. J. TWIST Activation by Hypoxia Inducible Factor-1 (HIF-1): Implications in Metastasis and Development. *Cell Cycle* **2008**, *7*, 2090–2096.
  17. Miyake, S.; Kitajima, Y.; Nakamura, J.; Kai, K.; Yanagihara, K.; Tanaka, T.; Hiraki, M.; Miyazaki, K.; Noshiro, H. HIF-1α Is a Crucial Factor in the Development of Peritoneal Dissemination via Natural Metastatic Routes in Scirrhous Gastric Cancer. *Int. J. Oncol.* **2013**, *43*, 1431–1440.
  18. Akakura, N.; Kobayashi, M.; Horiuchi, I.; Suzuki, A.; Wang, J.; Chen, J.; Niizeki, H.; Kawamura, K.; Hosokawa, M.; Asaka, M. Constitutive Expression of Hypoxia-Inducible Factor-1α Renders Pancreatic Cancer Cells Resistant to Apoptosis Induced by Hypoxia and Nutrient Deprivation. *Cancer Res.* **2001**, *61*, 6548–6554.
  19. Hu, H. T.; Ma, Q. Y.; Zhang, D.; Shen, S. G.; Han, L.; Ma, Y. D.; Li, R. F.; Xie, K. P. HIF-1α Links β-Adrenoceptor Agonists and Pancreatic Cancer Cells Under Normoxic Condition. *Acta Pharmacol. Sin.* **2010**, *31*, 102–110.
  20. Balasenthil, S.; Gururaj, A. E.; Talukder, A. H.; Bagheri-Yarmand, R.; Arrington, T.; Haas, B. J.; Braisted, J. C.; Kim, I.; Lee, N. H.; Kumar, R. Identification of Pax5 as a Target of MTA1 in B-Cell Lymphomas. *Cancer Res.* **2007**, *67*, 7132–7138.
  21. Nagaraj, S. R.; Shilpa, P.; Rachaiah, K.; Salimath, B. P. Cross-talk between VEGF and MTA1 Signaling Pathways Contribute to Aggressiveness of Breast Carcinoma. *Mol. Carcinog.* **2015**, *54*, 333–350.
  22. Li, Y.; Chao, Y.; Fang, Y.; Wang, J.; Wang, M.; Zhang, H.; Ying, M.; Zhu, X.; Wang, H. MTA1 Promotes the Invasion and Migration of Non-Small Cell Lung Cancer Cells by Down-regulating miR-125b. *J. Exp. Clin. Cancer Res.* **2013**, *32*, 33–39.
  23. Pakala, S. B.; Rayala, S. K.; Wang, R. A.; Ohshiro, K.; Mudvari, P.; Reddy, S. D.; Zheng, Y.; Pires, R.; Casimiro, S.; Pillai, M. R.; et al. MTA1 Promotes STAT3 Transcription and Pulmonary Metastasis in Breast Cancer. *Cancer Res.* **2013**, *73*, 3761–3770.
  24. Sankaran, D.; Pakala, S. B.; Nair, V. S.; Sirigiri, D. N.; Cyanam, D.; Ha, N. H.; Li, D. Q.; Santhoshkumar, T. R.; Pillai, M. R.; Kumar, R. Mechanism of MTA1 Protein Overexpression-Linked Invasion: MTA1 Regulation of Hyaluronan-Mediated Motility Receptor (HMMR) Expression and Function. *J. Biol. Chem.* **2012**, *287*, 5483–5491.
  25. Gururaj, A. E.; Singh, R. R.; Rayala, S. K.; Holm, C.; den Hollander, P.; Zhang, H.; Balasenthil, S.; Talukder, A. H.; Landberg, G.; Kumar, R. MTA1, A Transcriptional Activator of Breast Cancer Amplified Sequence 3. *Proc. Natl. Acad. Sci. U.S.A.* **2006**, *103*, 6670–6675.
  26. Iguchi, H.; Imura, G.; Toh, Y.; Ogata, Y. Expression of MTA1, A Metastasis-Associated Gene with Histone Deacetylase Activity in Pancreatic Cancer. *Int. J. Oncol.* **2000**, *16*, 1211–1214.
  27. Mariadason, J. M. HDACs and HDAC Inhibitors in Colon Cancer. *Epigenetics* **2008**, *3*, 28–37.
  28. Kim, Y. J.; Greer, C. B.; Cecchini, K. R.; Harris, L. N.; Tuck, D. P.; Kim, T. H. HDAC Inhibitors Induce Transcriptional Repression of High Copy Number Genes in Breast Cancer through Elongation Blockade. *Oncogene* **2013**, *32*, 2828–2835.
  29. Khan, O.; La Thangue, N. B. HDAC Inhibitors in Cancer Biology: Emerging Mechanisms and Clinical Applications. *Immunol. Cell Biol.* **2012**, *90*, 85–94.
  30. Huang, X.; Gao, L.; Wang, S.; Lee, C. K.; Ordentlich, P.; Liu, B. HDAC Inhibitor SNDX-275 Induces Apoptosis in ErbB2-Overexpressing Breast Cancer Cells via Down-Regulation of ErbB3 Expression. *Cancer Res.* **2009**, *69*, 8403–8411.
  31. Damaskos, C.; Karatzas, T.; Nikolidakis, L.; Kostakis, I. D.; Karamaroudis, S.; Boutsikos, G.; Damaskou, Z.; Kostakis, A.; Kourakis, G. Histone Deacetylase (HDAC) Inhibitors: Current Evidence for Therapeutic Activities in Pancreatic Cancer. *Anticancer Res.* **2015**, *35*, 3129–3135.
  32. Schneider, G.; Kramer, O. H.; Saur, D. A ZEB1-HDAC Pathway Enters the Epithelial to Mesenchymal Transition World in Pancreatic Cancer. *Gut* **2012**, *61*, 329–330.
  33. Mehdi, O.; Françoise, S.; Sofia, C. L.; Urs, G.; Kevin, Z.; Bernard, S.; Igor, S.; Anabela, C. D.; Dominique, L.; Eric, M.; et al. HDAC Gene Expression in Pancreatic Tumor Cell Lines Following Treatment with the HDAC Inhibitors Panobinostat (LBH589) and Trichostatin (TSA). *Pancreatology* **2012**, *12*, 146–155.
  34. Lehmann, A.; Denkert, C.; Budczies, J.; Buckendahl, A. C.; Darb-Esfahani, S.; Noske, A.; Muller, B. M.; Bahra, M.; Neuhaus, P.; Dietel, M.; et al. High Class I HDAC Activity and Expression Are Associated with RelA/p65 Activation in Pancreatic Cancer *in Vitro* and *in Vivo*. *BMC Cancer* **2009**, *9*, 395–404.
  35. De Souza, C.; Chatterji, B. P. HDAC Inhibitors as Novel Anti-cancer Therapeutics. *Recent Pat. Anti-Cancer Drug Discovery* **2015**, *10*, 145–162.
  36. Lin, K. T.; Wang, Y. W.; Chen, C. T.; Ho, C. M.; Su, W. H.; Jou, Y. S. HDAC Inhibitors Augmented Cell Migration and Metastasis through Induction of PKCs Leading to Identification of Low Toxicity Modalities for Combination Cancer Therapy. *Clin. Cancer Res.* **2012**, *18*, 4691–4701.
  37. Wagner, J. M.; Hackanson, B.; Lubbert, M.; Jung, M. Histone Deacetylase (HDAC) Inhibitors in Recent Clinical Trials for Cancer Therapy. *Clin. Epigenet.* **2010**, *1*, 117–136.
  38. Chen, S.; Sang, N. Histone Deacetylase Inhibitors: The Epigenetic Therapeutics That Repress Hypoxia-Inducible Factors. *J. Biomed. Biotechnol.* **2011**, *2011*, 197946.
  39. Liu, T.; Kuljaca, S.; Tee, A.; Marshall, G. M. Histone Deacetylase Inhibitors: Multifunctional Anticancer Agents. *Cancer Treat. Rev.* **2006**, *32*, 157–165.
  40. Yin, J. J.; Lao, F.; Fu, P. P.; Wamer, W. G.; Zhao, Y.; Wang, P. C.; Qiu, Y.; Sun, B.; Xing, G.; Dong, J.; et al. The Scavenging of Reactive Oxygen Species and the Potential for Cell Protection by Functionalized Fullerene Materials. *Biomaterials* **2009**, *30*, 611–621.
  41. Wang, J.; Chen, C.; Li, B.; Yu, H.; Zhao, Y.; Sun, J.; Li, Y.; Xing, G.; Yuan, H.; Tang, J.; et al. Antioxidative Function and Biodistribution of  $[Gd@C_{82}(OH)_{22}]_n$  Nanoparticles in Tumor-Bearing Mice. *Biochem. Pharmacol.* **2006**, *71*, 872–881.
  42. Kang, S. G.; Zhou, G.; Yang, P.; Liu, Y.; Sun, B.; Huynh, T.; Meng, H.; Zhao, L.; Xing, G.; Chen, C.; et al. Molecular Mechanism of Pancreatic Tumor Metastasis Inhibition by  $Gd@C_{82}(OH)_{22}$  and Its Implication for *De Novo* Design of Nanomedicine. *Proc. Natl. Acad. Sci. U.S.A.* **2012**, *109*, 15431–15436.
  43. Meng, J.; Liang, X.; Chen, X.; Zhao, Y. Biological Characterizations of  $[Gd@C_{82}(OH)_{22}]_n$  Nanoparticles as Fullerene Derivatives for Cancer Therapy. *Integr. Biol.* **2013**, *5*, 43–47.
  44. Ushio-Fukai, M.; Alexander, R. W. Reactive Oxygen Species as Mediators of Angiogenesis Signaling: Role of NAD(P)H Oxidase. *Mol. Cell. Biochem.* **2004**, *264*, 85–97.
  45. Xia, C.; Meng, Q.; Liu, L. Z.; Rojanasakul, Y.; Wang, X. R.; Jiang, B. H. Reactive Oxygen Species Regulate Angiogenesis and Tumor Growth through Vascular Endothelial Growth Factor. *Cancer Res.* **2007**, *67*, 10823–10830.
  46. Akakura, N. Significance of Constitutive Expression of Hypoxia-Inducible Factor-1 alpha (HIF-1α) Protein in Pancreatic Cancer. *Hokkaido Igaku Zasshi* **2001**, *76*, 375–384.
  47. Blum, R.; Kloog, Y. Metabolism Addiction in Pancreatic Cancer. *Cell Death Dis.* **2014**, *5*, e1065.
  48. Afanas'ev, I. Reactive Oxygen Species Signaling in Cancer: Comparison with Aging. *Aging Dis.* **2011**, *2*, 219–230.
  49. Liu, Y.; Chen, C.; Qian, P.; Lu, X.; Sun, B.; Zhang, X.; Wang, L.; Gao, X.; Li, H.; Chen, Z.; et al. Gd-Metallofullerenol Nanomaterial as Non-toxic Breast Cancer Stem Cell-Specific Inhibitor. *Nat. Commun.* **2015**, *6*, 5988.
  50. Yin, J. J.; Lao, F.; Meng, J.; Fu, P. P.; Zhao, Y.; Xing, G.; Gao, X.; Sun, B.; Wang, P. C.; Chen, C.; et al. Inhibition of Tumor Growth by Endohedral Metallofullerenol Nanoparticles

- Optimized as Reactive Oxygen Species Scavenger. *Mol. Pharmacol.* **2008**, *74*, 1132–1140.
51. Chen, C.; Xing, G.; Wang, J.; Zhao, Y.; Li, B.; Tang, J.; Jia, G.; Wang, T.; Sun, J.; Xing, L.; et al. Multihydroxylated  $[Gd@C_{82}(OH)_{22}]_n$  Nanoparticles: Antineoplastic Activity of High Efficiency and Low Toxicity. *Nano Lett.* **2005**, *5*, 2050–2057.
52. Tsaur, I.; Hudak, L.; Makarevic, J.; Juengel, E.; Mani, J.; Borgmann, H.; Gust, K. M.; Schilling, D.; Bartsch, G.; Nelson, K.; et al. Intensified Antineoplastic Effect by Combining an HDAC-Inhibitor, an mTOR-Inhibitor and Low Dosed Interferon alpha in Prostate Cancer Cells. *J. Cell. Mol. Med.* **2015**, 10.1111/jcmm.12583.
53. Joseph, J.; Mudduluru, G.; Antony, S.; Vashistha, S.; Ajitkumar, P.; Somasundaram, K. Expression Profiling of Sodium Butyrate (NaB)-Treated Cells: Identification of Regulation of Genes Related to Cytokine Signaling and Cancer Metastasis by NaB. *Oncogene* **2004**, *23*, 6304–6315.
54. Zgouras, D.; Wachtershauser, A.; Frings, D.; Stein, J. Butyrate Impairs Intestinal Tumor Cell-Induced Angiogenesis by Inhibiting HIF-1 $\alpha$  Nuclear Translocation. *Biochem. Biophys. Res. Commun.* **2003**, *300*, 832–838.
55. Lee, Y. M.; Kim, S. H.; Kim, H. S.; Son, M. J.; Nakajima, H.; Kwon, H. J.; Kim, K. W. Inhibition of Hypoxia-Induced Angiogenesis by FK228, a Specific Histone Deacetylase Inhibitor, via Suppression of HIF-1 $\alpha$  Activity. *Biochem. Biophys. Res. Commun.* **2003**, *300*, 241–246.
56. Kim, M. S.; Kwon, H. J.; Lee, Y. M.; Baek, J. H.; Jang, J. E.; Lee, S. W.; Moon, E. J.; Kim, H. S.; Lee, S. K.; Chung, H. Y.; et al. Histone Deacetylases Induce Angiogenesis by Negative Regulation of Tumor Suppressor Genes. *Nat. Med.* **2001**, *7*, 437–443.
57. Jeong, S. G.; Cho, G. W. Trichostatin A Modulates Intracellular Reactive Oxygen Species through SOD2 and FOXO1 in Human Bone Marrow-Mesenchymal Stem Cells. *Cell Biochem. Funct.* **2015**, *33*, 37–43.
58. Du, J.; Zhang, L.; Zhuang, S.; Qin, G. J.; Zhao, T. C. HDAC4 Degradation Mediates HDAC Inhibition-Induced Protective Effects against Hypoxia/Reoxygenation Injury. *J. Cell. Physiol.* **2015**, *230*, 1321–1331.
59. Zuo, G.; Huang, Q.; Wei, G.; Zhou, R.; Fang, H. Plugging into Proteins: Poisoning Protein Function by a Hydrophobic Nanoparticle. *ACS Nano* **2010**, *4*, 7508–7514.
60. Zuo, G.; Zhou, X.; Huang, Q.; Fang, H.; Zhou, R. Adsorption of Villin Headpiece onto Graphene, Carbon Nanotube, and C60: Effect of Contacting Surface Curvatures on Binding Affinity. *J. Phys. Chem. C* **2011**, *115*, 23323–23328.
61. Tsai, H.-C.; Baylin, S. B. Cancer Epigenetics: Linking Basic Biology to Clinical Medicine. *Cell Res.* **2011**, *21*, 502–517.
62. Lee, K. J.; Lee, K. Y.; Lee, Y. M. Downregulation of a Tumor Suppressor RECK by Hypoxia through Recruitment of HDAC1 and HIF-1 $\alpha$  to Reverse HRE Site in the Promoter. *Biochim. Biophys. Acta* **2010**, *1803*, 608–616.
63. Millard, C. J.; Watson, P. J.; Celardo, I.; Gordiyenko, Y.; Cowley, S. M.; Robinson, C. V.; Fairall, L.; Schwabe, J. W. Class I HDACs Share a Common Mechanism of Regulation by Inositol Phosphates. *Mol. Cell* **2013**, *51*, 57–67.
64. Zhou, G.; Li, Y.; Liu, Y.; Ge, C.; Li, W.; Sun, B.; Li, B.; Gao, Y.; Chen, C. Subcellular Distribution of Polyhydroxylated Metallofullerene  $Gd@C_{82}(OH)_{22}$  in Different Tissues of Tumor-Bearing Mice. *J. Nanosci. Nanotechnol.* **2010**, *10*, 8597–8602.
65. Zhang, M.; Xing, G.; Yuan, H.; Chang, X.; Jing, L.; Zhao, Y.; Zhu, C.; Fang, X. Transmembrane Delivery of Aggregated  $[Gd@C_{82}(OH)_{22}]_n$  Nanoparticles. *J. Nanosci. Nanotechnol.* **2010**, *10*, 8556–8561.
66. Hait, N. C.; Allegood, J.; Maceyka, M.; Strub, G. M.; Harikumar, K. B.; Singh, S. K.; Luo, C.; Marmorstein, R.; Kordula, T.; Milstien, S.; et al. Regulation of Histone Acetylation in the Nucleus by Sphingosine-1-Phosphate. *Science* **2009**, *325*, 1254–1257.
67. Zheng, L. N.; Wang, M.; Zhao, L. C.; Sun, B. Y.; Wang, B.; Chen, H. Q.; Zhao, Y. L.; Chai, Z. F.; Feng, W. Y. Quantitative Analysis of  $Gd@C_{82}(OH)_{22}$  and Cisplatin Uptake in Single Cells by Inductively Coupled Plasma Mass Spectrometry. *Anal. Bioanal. Chem.* **2015**, *407*, 2383–2391.